Proceedings of the ASME 2010 3rd Joint US-European Fluids Engineering Summer Meeting and 8th International Conference on Nanochannels, Microchannels, and Minichannels
FEDSM-ICNMM2010
August 1-5, 2010, Montreal, Canada

FEDSM-ICNMM2010-30298

A VALIDATION DATABASE FOR FLOW IN A PARALLEL TRIANGULAR HEAT EXCHANGER TUBE ARRAY

John Mahon *
School of Engineering
Trinity College Dublin
Dublin, Ireland
Email: mahonjp@tcd.ie

Craig Meskell
School of Engineering
Trinity College Dublin
Dublin, Ireland
Email: cmeskell@tcd.ie

ABSTRACT

An experimental parametric study of the surface pressure on a cylinder in the sixth row of a rotated triangular tube array (P/d=1.375) with air cross flow has been conducted. A range of static displacements were examined. Jet switching was observed in this array and resulted in the large asymmetry observed in the pressure distribution around the static cylinder even in a geometrically symmetric configuration. The large fluctuations in lift force due to jet switching suggest that it should be more seriously considered when designing against fatigue failure. The effect of jet switching on the pressure distribution data was mitigated by deconstructing the pressure distribution into two modes. Forces were calculated from the pressure measurements offering an insight into the fluid mechanics generating the forces. No simple parameterisation was found for either the lift or drag force, but it was found that the drag force was only weakly affected by the tube displacement. The dataset presented here compliments the data previously presented for normal triangular arrays and represents a valuable reference for validation of simulations and flow-induced vibration models.

NOMENCLATURE

C_D	Drag coefficient
C_L	Lift coefficient
C_P	Mean pressure coefficient
d	Tube diameter
F_D	Drag Force
F_L	Lift force
FEI	Fluidelastic instability
l	Tube length
P	Pitch
P/d	Pitch ratio
P_θ	Mean pressure at a give position angle
P_0	Mean pressure at stagnation point
Re	Reynolds number
RT	Rotated triangular
U	Free stream flow velocity
U_g	Gap velocity
y/d	Non-dimensionalised tube displacement (y^*)
θ	Position angle
ρ	Fluid density (air)

INTRODUCTION

In 1979 Paidoussis (1) presented details on case studies of flow induced vibration problems in heat exchangers and nuclear reactors. We are interested in the 33 cases presented on flow induced vibration due to a cross-flow. The flow induced vibration mechanisms were classified under a number of headings: vortex shedding; vortex shedding and acoustic resonance; fluidelas-

*Address all correspondence to this author.

tic instability; turbulent buffeting; and unknown. It is generally accepted that the mechanism of fluidelastic instability has the greatest potential to cause damage and it occurs when a critical velocity is reached. The mechanism has the potential to destroy a unit in a number of hours. As such the operating cross-flow velocity chosen is on the conservative side compared to the fluidelastic threshold, or so its thought. However, as the fluid mechanics are not fully understood it is difficult to determine whether cross-flow velocity is conservative or not even if the cross-flow velocity does not cause the onset of fluidelastic instability.

The mechanism responsible for fluidelastic instability (FEI) in tube arrays has been described by three theoretical frameworks: the "wavy-wall" model (Lever & Weaver (2)); the quasi-static model (Connors (3)); and the quasi-steady model (Price & Paidoussis (4)). There are also a number of empirical models. In addition, there have been a number of numerical simulations of flow through heat exchangers tube arrays and fluideleastic instability using Large Eddy Simulation, Reynolds Averaged Navier Stokes and vortex methods (e.g. (5), (6), (7)). These models, whether semi-empirical or numerical, are based on very different assumptions of the fluid mechanics. However, the approach for validating these models depends primarily on comparison of predicted critical velocity to experimental values. Unfortunately, while this threshold is ultimately of greatest interest from a practical point of view, the experimental data available show a significant unexplained scatter and hence confidence in model validation is poor. In order to provide an initial validation of the assumptions and predictions of these models, a detailed survey of the surface pressure distribution on a statically displaced cylinder in a rotated triangular tube array has been conducted. While there is already limited pressure data in the literature ((8), (9), (10)), pressure distributions were measured for only a few Reynolds numbers. Furthermore, until recently there have been no comprehensive studies of the pressure field around a statically displaced cylinder within a tube array available. Batham (11) presented a limited study of the pressure distribution around a statically displaced cylinder in an array. The configuration used was a ten row in-line array with pitch ratio of 1.25. It was report that the first three rows where displaced by 0.25mm which corresponds $\sim 0.5\%$ tube displacement and that the pressure distribution "completely changed". However no detailed results were presented. More recently, Mahon & Meskell (12) presented pressure distributions around a cylinder in three normal triangular tube arrays, for a range of Reynolds number and static tube displacements[1]. Nonetheless, there is still limited information on parallel (rotated) triangular tube arrays. This study presents a survey of surface pressure in a parallel triangular tube array with static tube displacement.

As detailed above, models for fluidelastic instability tend to look at the critical velocity and this is not unreasonable given that the critical velocity is generally the quantity of interest when one is looking to predict the onset of fluidelastic instability. However, there is significant scatter in the threshold velocities presented in the literature. It would therefore be beneficial to be able to validate the models using a number of intermediate steps. The data presented in this paper provides that intermediate step. Consider the quasi-steady model, this model separates the fluidelastic force into a magnitude dependant on the static fluid force and a phase dependent on the time delay. In the magnitude dependent part, the fluid forces (lift and drag) are assumed to be identical to those measured with the tube at rest in the same location (this is the quasi-static assumption). Using the data presented in this study it is possible to validate the magnitude dependent part of the model.

EXPERIMENTAL SETUP

The experimental facility consists of a draw down wind tunnel which has a tube array installed in the test section. The test-section is 750 mm long with a cross-section of 300 mm high $\times$ 272 mm wide. An 8 row rotated triangular array with a pitch ratio of 1.375 and air cross flow was investigated in this study. A schematic of the test-section is shown in Fig. 1.

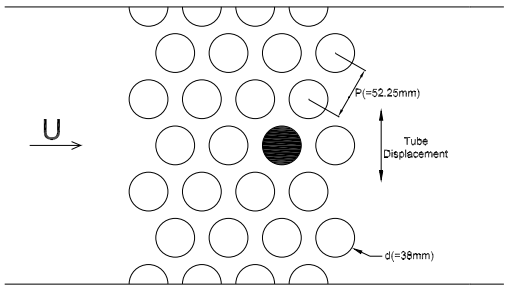

FIGURE 1. Test section schematic: parallel triangular array, P/d=1.375

A pitot-static tube installed upstream of the tube array connected to a Furness Control micromanometer (model FC015) measured the free stream flow velocity in the test section. The flow velocity in the wind tunnel test-section ranged from 2 m/s to 10 m/s with a free stream turbulence intensity of less than 1%. The tubes in the array (38 mm diameter) are rigidly fixed, except for one tube which will be referred to as the instrumented cylinder.

The instrumented cylinder has 36 pressure taps with a diameter of 1 mm and located at the mid-span around the circumference of the cylinder (equispaced at 10^o intervals). The length of the cylinder assembly within the test section was 298 mm with a diameter of 38 mm.

[1]This data is available at http://www.ercoftac.org

The instrumented tube was connected to the pressure transducers with short lengths of 2 mm internal diameter silicone tubing. Each pressure tap was monitored with a differential pressure transducer (Honeywell 164PC01D37). The other port of the pressure transducer was vented to atmosphere. In effect the gauge pressure was measured.

The signal from the pressure transducer was acquired simultaneously at a sample frequency of 1024 Hz. As the primary focus of this study is the mean pressure distribution, the pressure transducers were calibrated by applying a constant known pressure. From this, the sensitivity of the pressure transducer was obtained. i.e. a relationship between the output voltage from the pressure transducer at a known pressure. The other pressure transducers were then calibrated with respect to this reference pressure transducer. The readings from the pressure transducers were digitised and logged using a NI 48 channel, 24 bit data acquisition frame. Each channel was simultaneously sampled and automatically low pass filtered to avoid aliasing.

The tube was mounted on a traverse (located outside the wind tunnel) allowing a specific static displacement to be applied to the cylinder. The traverse facilitated fine displacements and the displacement was monitored with a clock gauge with an accuracy of up to 0.01 mm. Additional information on the test setup including schematics and photographs of the pressure tap tube can be found in Mahon & Meskell (12) and Mahon (13).

RESULTS

An 8 row rotated triangular array with a pitch ratio of 1.375 with air cross flow was investigated. Surface pressure measurements on a cylinder in the center of the sixth row have been obtained for a range of flow velocities and static tube displacements. Table 1 details the free stream velocities tested as well as the associated gap velocities and Reynolds numbers (Reynolds numbers are based on the gap velocity) while Table 2 outlines the tube displacements tested.

The pressure distribution around the cylinder was non-dimensionalised and the results presented in terms of the mean pressure coefficient. The pressure coefficient, C_P, was defined as

$$C_P = 1 - \frac{P_o - P_\theta}{\frac{1}{2}\rho U_g^2}, \qquad (1)$$

where P_o refers to the mean pressure at the stagnation point, P_θ refers to the local mean static pressure at a given angular distance (also referred to as position angle) and is defined as the positive clockwise angle starting from the front of the cylinder (see Fig. 2), U_g is the gap velocity ($U_g = U[P/(P-d)]$) and ρ is the fluid density. The pressure coefficient was expressed in this way as taking the free stream static pressure as the reference pressure was not appropriate as the mean static pressure varies throughout the array. The experimental setup has been validated previously (Mahon & Meskell (12)) by measuring the mean pressure distribution around an isolated cylinder and comparing the results with those in the literature. The curve compared well with data in the literature e.g. Zukauskas (14).

TABLE 1. Free stream velocities (U), gap velocities (U_g) and Reynolds numbers (Re) tested

U (m/s)	U_g (m/s)	Re $(\times 10^4)$
2	7.3	1.97
3	11.0	2.95
4	14.7	3.93
5	18.3	4.91
6	22.0	5.90
7	25.7	6.88
8	29.3	7.86
9	33.0	8.84
10	36.7	9.83

TABLE 2. Tube displacements tested

y/d (%)	0	1	3	5	7	10	-5

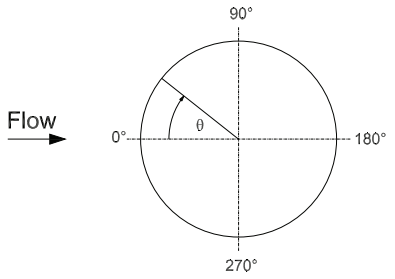

FIGURE 2. Schematic of position angle

Pressure Distribution

Figure 3 shows the mean pressure distribution around a cylinder in the sixth row of a parallel (rotated) triangular tube array with zero static displacement. It is apparent that the pressure distribution is not symmetric. The asymmetry was significantly larger than that associated with a rotational offset in the position

angle. It is possible that the the misalignment in the tubes' position resulted in the asymmetry distribution, but the misalignment would have to be very large. When the tests were repeated the pressure distribution changed. This behaviour was also observed at other flow velocities. Hence, the authors are satisfied that the asymmetry in the pressure distribution was not as a result of misalignment. Mahon & Meskell (12) observed large asymmetry in one of the normal triangular arrays investigated and this was attributed to bistable flow structures. This effect has also been observed by others for example Zdravkovich & Stonebanks (15) and Zdravkovich (16).

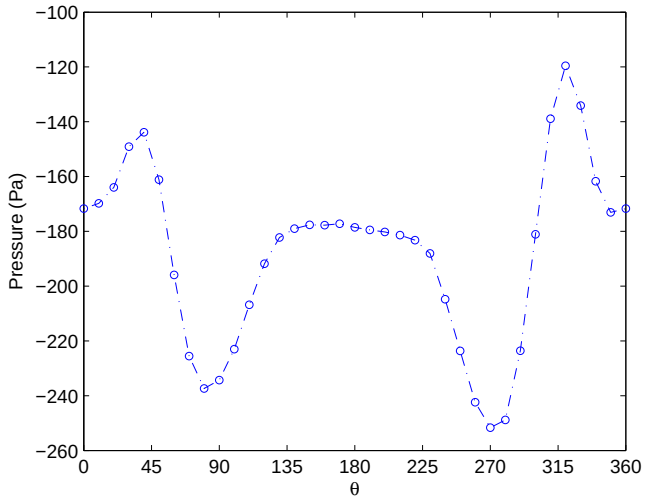

FIGURE 3. Mean pressure Distribution, y/d=0% and U=4m/s.

Further investigation reveals that there is bi-stable flow regime. Figure 4 shows the time resolved pressure signal at $\theta = 50^o$ and at a flow velocity of 4m/s. It is clear that there is significant variation in the pressure signal. Plotting a histogram of the signal (Fig. 5) it is apparent that there is a bi-modal flow instability (jet switching). This bi-modal behaviour was observed at most flow velocities and tube displacements tested with the exception of the flow velocity at 2 and 3m/s. It is possible that flow instability was occurring at those velocities but it was not as pronounced as in the other cases.

The presence of a bi-modal flow instability (jet switching) complicates the analysis of the data as the pressure distribution changes from test to test regardless of whether the velocity or displacement parameters are changed.

As mentioned previously the flow instability (jet switching) observed was bi-modal. In an attempt to obtain a better behaved data set, an analysis to minimise the effect of jet switching was employed and is described below. It was generally found that only two modes exist. If the time record was sufficiently long

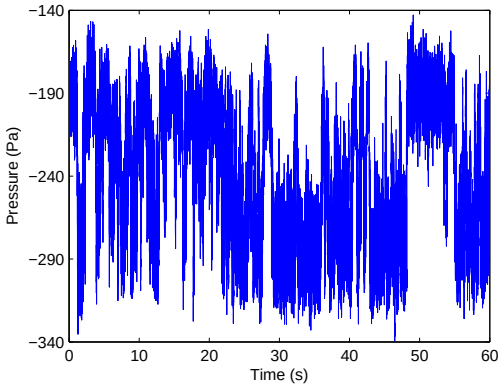

FIGURE 4. Time resolved pressure at θ=50^o 11 y/d=0% and U=5 m/s

the mean pressure distribution would be unbiased. However, as the jet switching is a random intermittent phenomenon with a temporal spacing of tens of seconds, the record length would be prohibitive. Thus, the approach taken to generate the long term average was to decompose the pressure records into two modes, and to take the average of these two modes. Note that this does not remove the effect of jet switching; rather it offers the mean pressure distribution for the hypothetical case were it is equally likely that the jet is aligned on one side of the tube as the other. In order to illustrate this consider Fig. 5 which shows the data at $\theta = 50^o$. Figure 5 shows the histogram of the entire record for this position. The bimodal distribution is the effect of jet switching and is clearly visible. The two configurations of the flow are termed Mode 1 and Mode 2. These are not modes in a strict sense, as a linear combination is not possible, but rather refer to the instantaneous configuration of the flow field. Using the tapping which displays the most pronounced bi-modal characteristics, the time record of each pressure tap was characterised as either Mode 1 or Mode 2. Using this approach all the pressure signals can be decomposed into the two modes. Figure 6 shows the histogram of the pressure data at $\theta = 270^o$ with the separated modes. These modes were obtained using the data sets retrieved via mode separation at $\theta = 50^o$.

Fig. 7 shows the pressure distribution at the two modes. It is clear that the two flow field configurations associated with the two modes yield are antisymmetric. The pressure distributions from the two dominant jet switching modes were averaged. The pressure distribution with the bias of jet switching removed in this way is shown in Fig. 8. The pressure distribution is symmetric and is a significant improvement on the using a simple mean pressure distribution. In some instances the pressure distribution was still slightly asymmetric, however, in these cases there was still a significant improvement in symmetry of the pressure distribution when compared to the mean pressure distribution.

Examining the pressure distribution in greater detail at θ=30-40^o and 320-330^o the pressure is a maximum due to the

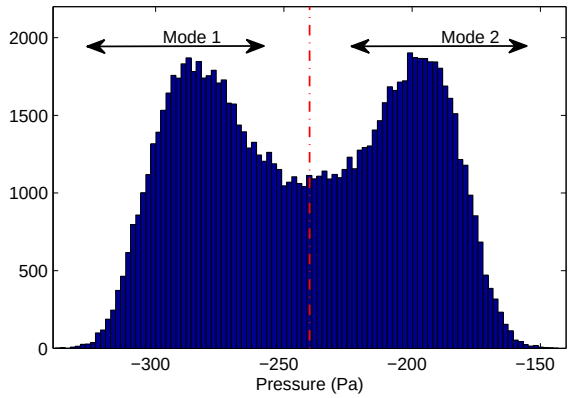

FIGURE 5. Histogram of pressure at θ=50^o, y/d=0% and U=5 m/s

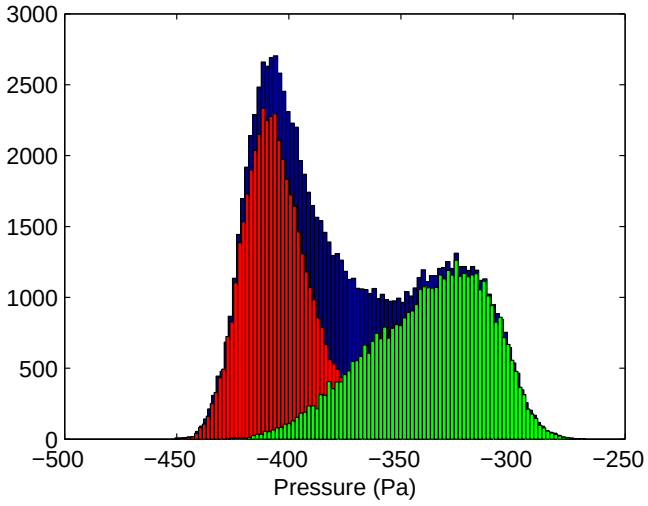

FIGURE 6. Histogram of pressure at $\theta = 270^o$, y/d=0% and U=5 m/s. Red - Mode 1, Green - Mode 2, Blue - Combination of both modes

flow from the upstream tubes impinging on to the tube (reattachment of the shear layers separated from the upstream tubes). The pressure decreases upon moving away from this region in both the upstream and downstream directions. Surprisingly, the pressure reaches a minimum at θ=90^o and 270^o, even though the minimum gap between adjacent cylinders is at $\pm$60^o and $\pm$120^o, suggesting that viscous losses play a role in the pressure distribution even before the large scale separation. After $\theta = \pm 130^o$ the flow separates, and results in the relatively constant pressure distribution at the rear of the cylinder.

Figure 9 plots the pressure distribution around the tube at y/d=0% for a range of Reynolds numbers. It is observed that the pressure distribution changes with Reynolds number. At Re$\approx 7\times10^4$ (U=7-8m/s) the locations of minimum and maxi-

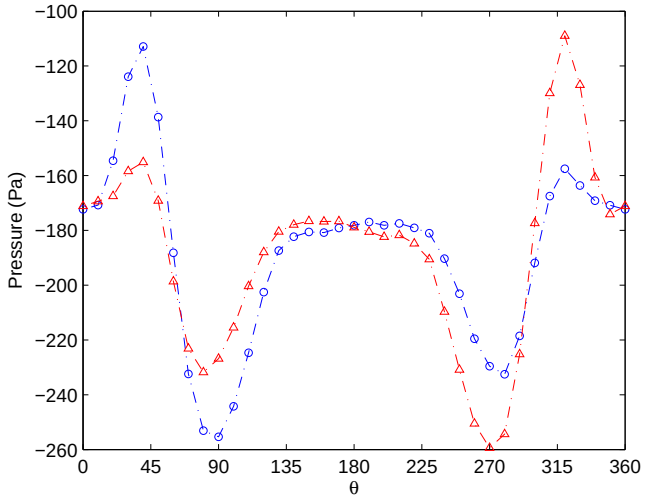

FIGURE 7. Mode 1 and Mode 2 of the pressure distribution, y/d=0% and U=4m/s

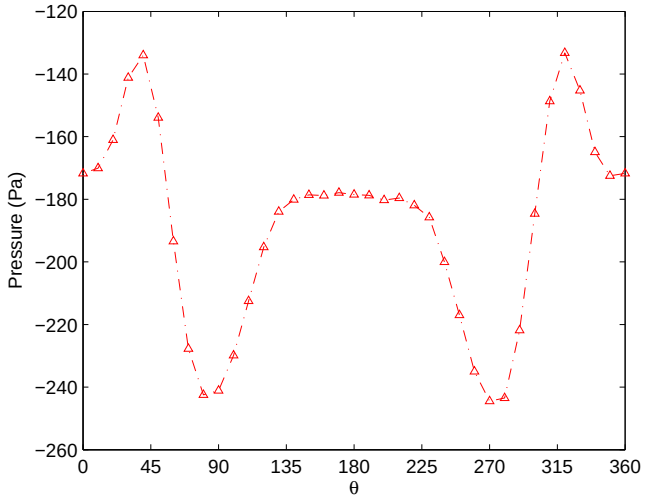

FIGURE 8. Mode average pressure distribution, y/d=0% and U=4m/s

mum pressure change suggesting a change in the flow pattern. Furthermore, at the rear of the cylinder the point of separation moves closer to the rear of the cylinder.

Tube displacement

Static tube displacements of 1%, 3%, 5%, 7% and 10% of tube diameter were examined. Figures 10, 11 and 12 show mode average pressure distribution around a cylinder in the sixth row for the range of static tube displacements at flow velocities of 4, 6 and 8m/s respectively. The effect of tube displacement is apparent. The region θ=30-40^o shows a decrease in pressure whereas the region θ=320-330^o on the opposite side of the cylinder shows

an increase in pressure. These effects get more pronounced as the tube displacement increases. The reason for the change in pressure is due to the reattachment of the shear layers separated from the upstream tubes. The region θ=320-330^o is shifted into the shear layer path from the upstream cylinder while the region θ=30-40^o on the opposite side moves away from the shear layer from the upstream cylinder.

At the top and bottom of the cylinder there is a significant change in the distribution with the pressure in the region θ=90^o reducing and the opposite occurring on the other side of the cylinder at θ=270^o. At the rear of the cylinder the pressure distribution becomes slightly skewed. This is due to the deflection of the separated region. However, this is a minor effect.

Fluid Forces

As the current study only measured pressure, the contribution of skin friction can not be assessed. However, in the current study, the lowest Reynolds number tested was greater than 2×10^4. At these Reynolds numbers, it is reasonable to assume that skin friction forces are small and can be neglected. Hence, the lift and drag forces are given by:

$$F_D = \int_0^{2\pi} Pdl\cos(\theta)d\theta, \tag{2}$$

$$F_L = \int_0^{2\pi} Pdl\sin(\theta)d\theta, \tag{3}$$

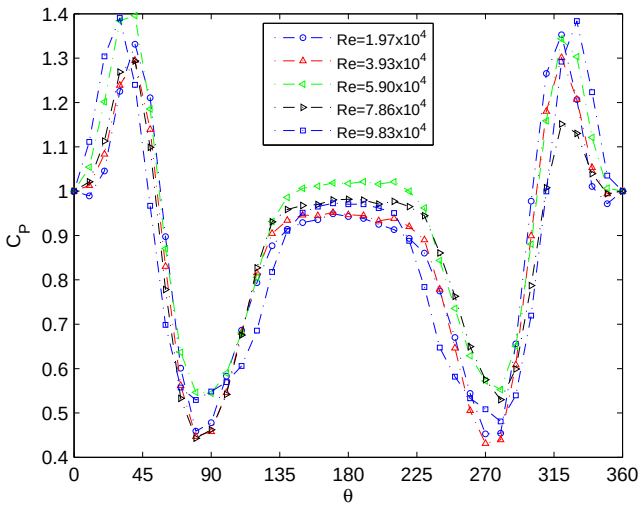

FIGURE 9. C_P at various Reynolds numbers, y/d=0%

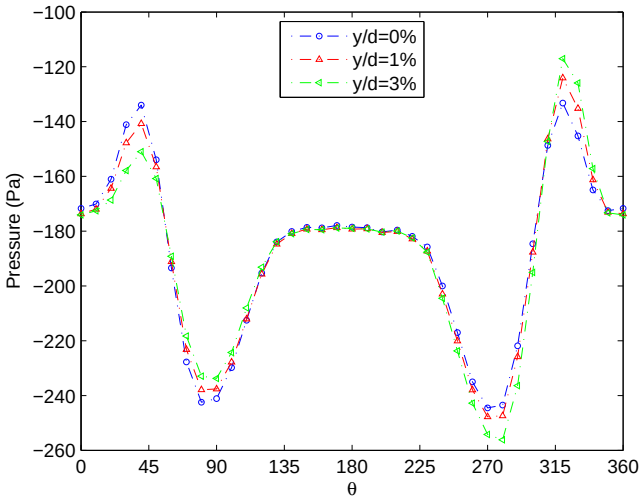

FIGURE 10. Mode average pressure distribution, U=4m/s.

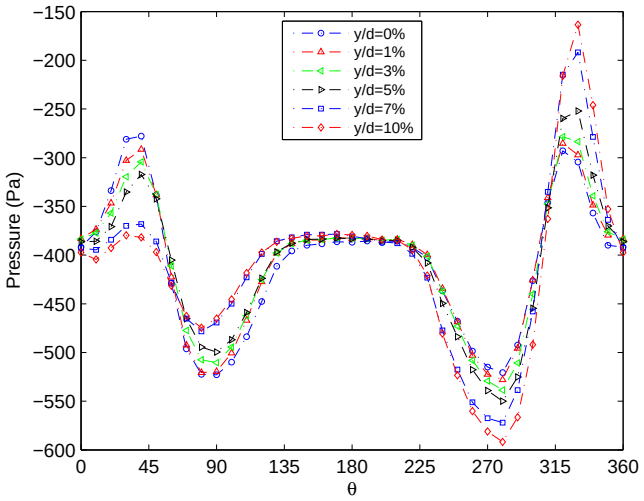

FIGURE 11. Mode average pressure distribution, U=6m/s.

Before examining the mean lift and drag forces on the cylinder for a range of flow velocities and tube displacements, it is interesting to consider the effect of the jet switching on the fluid forces. Figure 13(a) presents the time resolved lift force where it was observed that the lift force varied significantly over time. Furthermore, Fig. 13(b) shows that the lift force fluctuations were both positive and negative. As can be seen in Figs. 14(a) and (b), the effect of jet switching on the drag force was weak as demonstrated by the random fluctuations about a mean drag force and nearly Gaussian distribution.

It is interesting to note that Mahon *et al.* (17) have recently completed a preliminary investigation of the spanwise coherence in pressure in normal triangular arrays. There results strongly

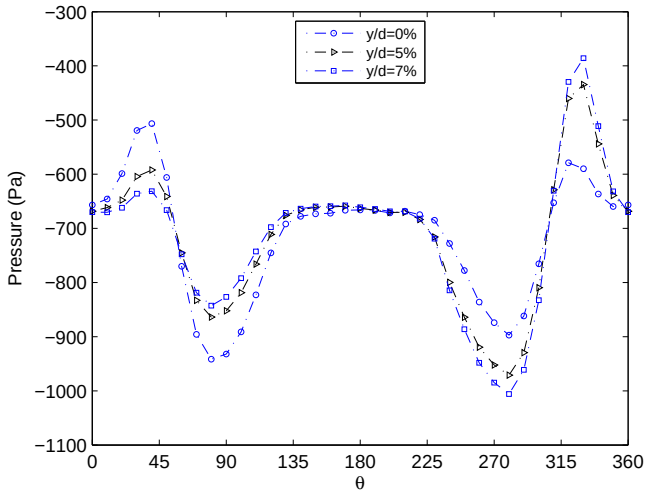

FIGURE 12. Mode average pressure distribution, U=8m/s.

suggest that variation in lift force due to the jet switching phenomenon will be correlated along the tube length. Hence, jet switching may be a significant issue for designers when estimating the fatigue life of a heat exchanger unit (i.e. when considering the wear rate due to turbulent buffeting).

Drag force

The drag force for the range of tube displacements collapses well as seen in Fig. 15. It was shown previously that there were substantial changes in the pressure distribution as a result of displacing the tube. These changes also occurred at position angles where there is a large contribution to the drag force. However, the net contribution to the drag force did not change significantly because the pressure increases occur on one side of the cylinder and the opposite occurs on the other side resulting in a flow redistribution rather than an overall change in the drag force. The drag force is reasonably well behaved increasing in magnitude with increasing velocity but no simple parameterisation in terms of velocity was found. At Re$\approx 7\times 10^4$ there is a change in the drag force behaviour, as observed in the pressure coefficient data presented above.

The drag force data is also presented in terms of the non-dimensioned drag coefficient,

$$C_D = \frac{F_D}{\frac{1}{2}\rho d l U_g^2}. \quad (4)$$

The average drag coefficient (for all tube displacements) is presented in Fig. 16 as function of Reynolds number. The change in trend around Re$\approx 7\times 10^4$ is still apparent.

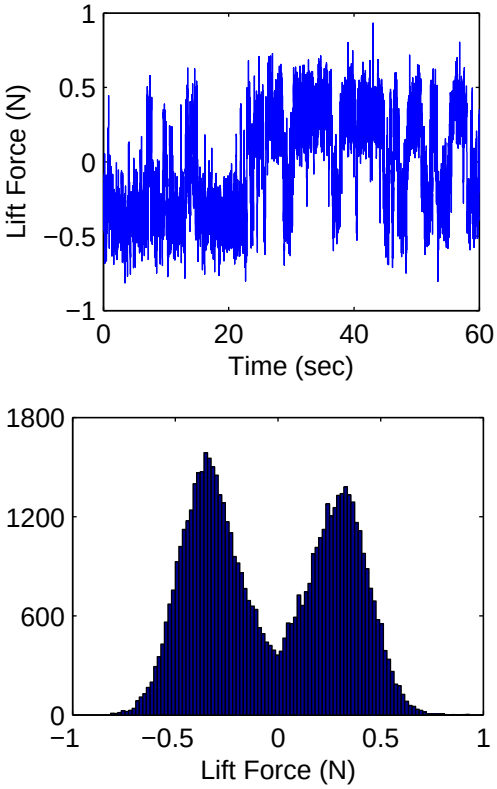

FIGURE 13. (a) Time resolved lift force y/d=0% and u=4 m/s (b) Histogram of the lift force y/d=0% and u=4 m/s

Lift force

The lift force around the cylinder in an array appears to be reasonably well behaved. When y/d=0% the lift force fluctuated around zero. When the tube was displaced, a net lift force in the direction opposite to the tube displacement results. The magnitude of the force generally increased with tube displacement and flow velocity. However, at Re$\approx 7\times 10^4$ this trend changes with the magnitude of the lift coefficient decreasing (Fig. 17) with increasing Reynolds number and at the highest Reynolds number observed the effect of displacement is minimal.

When the lift force and coefficient are split into the various modes Fig. 18 it becomes clear as to why the rate of the lift coefficient changes at the higher Reynolds number ranges. At the lower Reynolds numbers the slope of the lift coefficients for the two modes are similar. However, at the higher Reynolds numbers the slopes of the lift coefficient data set are not similar and the slopes differ. Furthermore, at the highest Reynolds number tested the slope of one mode is negative whilst the slope of the other mode is positive.

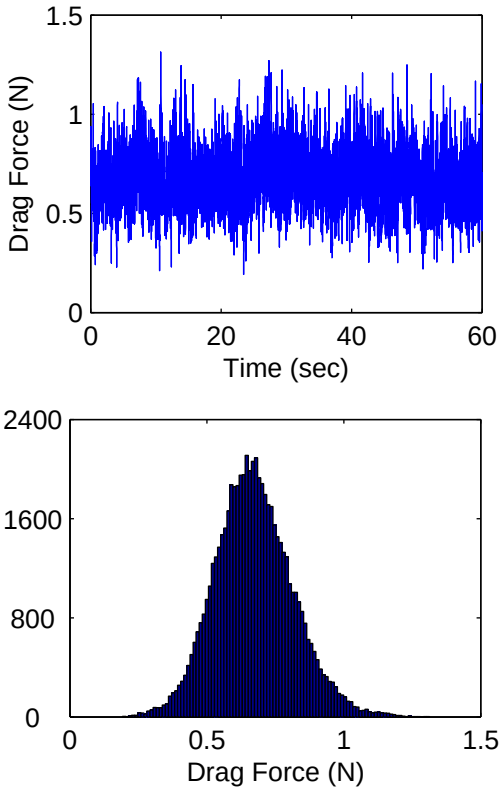

FIGURE 14. (a) Time resolved drag force y/d=0% and U=4 m/s (b) Histogram of the drag force y/d=0% and U=4 m/s

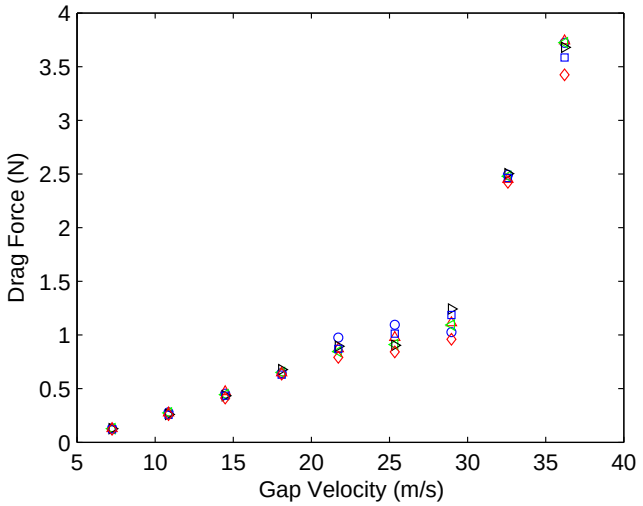

FIGURE 15. Drag force at all tube displacements: ○, y/d=0%; △, y/d=1%; ◁, y/d=3%; ▷, y/d=5%; □, y/d=7%; ◇, y/d=10%

Fluid force gradients

The onset of fluidelastic instability is determined primarily by the gradients of the fluid force. This can be seen most clearly in the quasi-steady and quasi-unsteady models of FEI, but is an implicit feature of the other models as well. Figures 19 & 20 show the variation of the force coefficient gradients at zero displacement with gap velocity.

It can be seen that dC_D/dy^* did not change significantly with gap velocity and is approximately zero, indicating that the drag coefficient is not sensitive to displacement, as previously noted. The magnitude of the lift curve slope, dC_L/dy^*, increases with gap velocity. However at the higher velocities the trend changes with the magnitude of dC_L/dy^* reducing. This change in trend occurred at Re=$\approx 7\times 10^4$ and coincides with the change in flow behaviour observed previously. This may imply that the fluidelastic behaviour of an array (i.e. the threshold velocity) will change as Reynolds number is increased, but further work is required to investigate this.

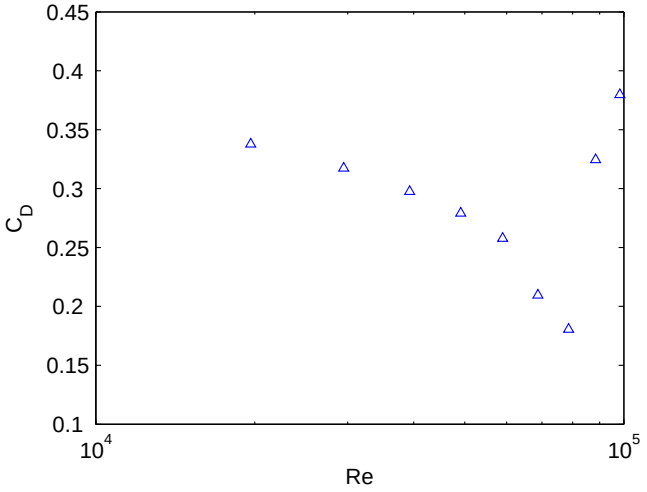

FIGURE 16. Average drag coefficient (C_D) variation with Reynolds number (Re)

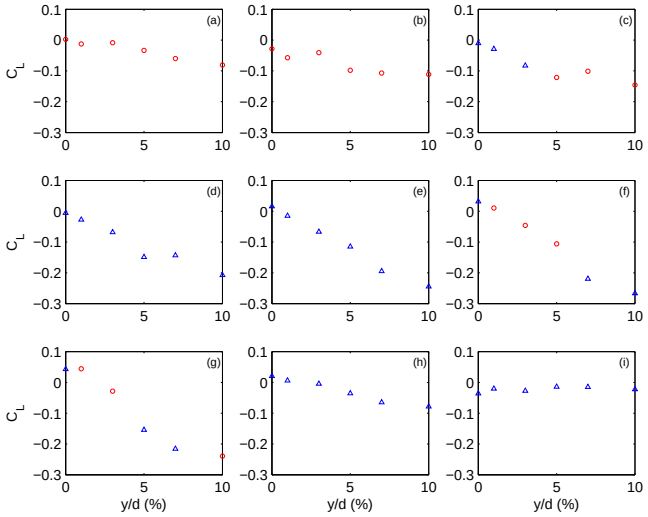

FIGURE 17. Lift Coefficient (C_L) variation with tube displacement for a range of flow velocities. C_L obtained using ○ - Mean pressure, △ - Mode average pressure. (a) U=2m/s; (b) U=3m/s (c) U=4m/s; (d) U=5m/s; (e) U=6m/s; (f) U=7m/s; (g) U=8m/s; (h) U=9m/s; (i) U= 10m/s

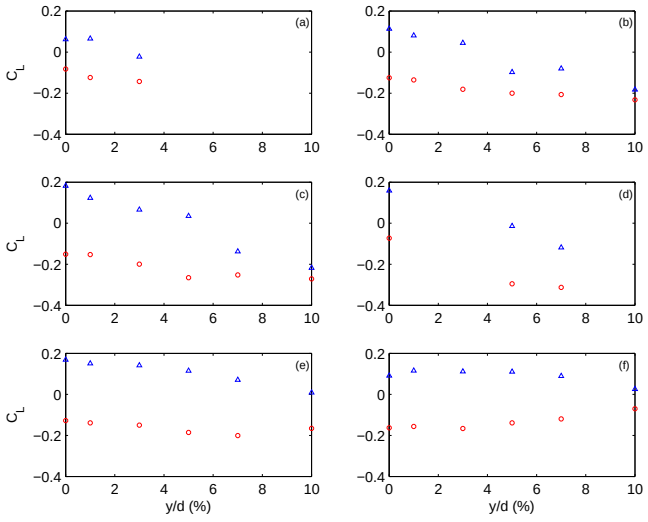

FIGURE 18. Lift coefficient decomposed into two modes; ○ - Mode 1, △ - Mode 2. (a) U=4m/s; (b) U=5m/s (c) U=6m/s; (d) U=8m/s; (e) U=9m/s; (f) U=10m/s

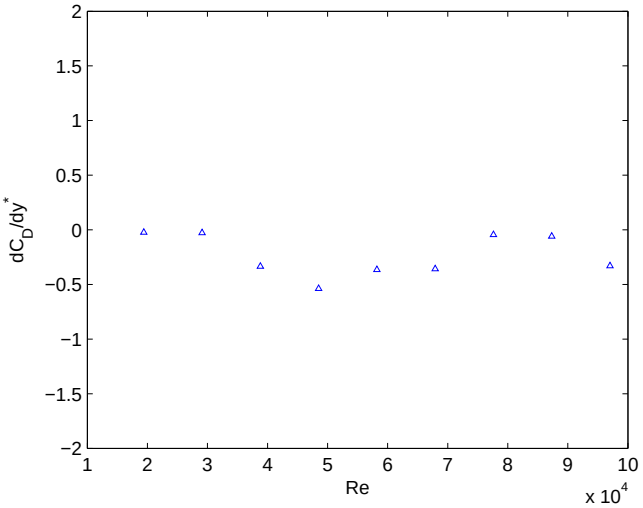

FIGURE 19. Drag coefficient gradient dC_D/dy^*

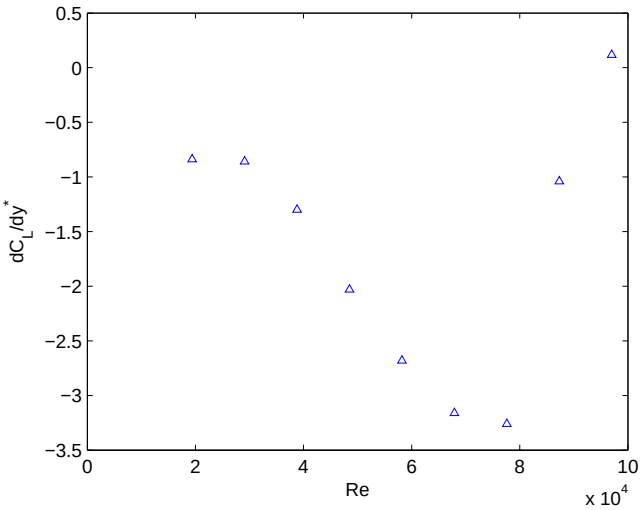

FIGURE 20. Lift coefficient gradient dC_L/dy^*

CONCLUSIONS

A parametric study of the surface pressure on a tube in a parallel triangular array P/d=1.375 has been conducted. The pressures often exhibit bi-modal, and this has been attributed to jet switching in the flow. The asymmetric effect of the jet switching has been controlled to provide an equivalent long term average pressure distribution around the cylinder for a range of flow velocities and displacements. It has been found that the behaviour of the fluid forces changes dramatically at a Reynolds of approximately 7×10^4. The database obtained provides a useful reference for validating both numerical simulations and semi-empirical models of flow induced vibration in tube arrays.

ACKNOWLEDGMENT

This publication has emanated from research conducted with the financial support of Science Foundation Ireland.

REFERENCES

[1] Paidoussis, M., 1979. "Flow-induced vibrations in nuclear reactors and heat exchangers. practical experiences and state of knowledge". *In E. Naudascher and D. Rockwell (Eds.), Practical experiences with flow-induced vibration*, pp. 1–56.

[2] Lever, J., and Weaver, D., 1986. "On the stability of heat exchanger tube bundles. part i: modified theoretical model. part ii: numerical results and comparison with experiment". *Journal of Sound and Vibration,* ***107***, pp. 375–410.

[3] Connors, H. J., 1970. "Fluid-elastic vibration of tube arrays excited by cross flow". *Proceedings, Flow-induced vibrations in heat exchangers, ASME, Chicago*, pp. 42–56.

[4] Price, S. J., and Paidoussis, M. P., 1984. "An improved mathematical model for the stability of cylinder rows subject to cross-flow". *Journal of Sound and Vibration,* ***97***(4), pp. 615–640.

[5] Kassera, V., Kacem-Hamouda, L., and Strohmeier, K., 1995. "Numerical simulations of flow induced vibrations of a tube bundle in uniform cross flow". In ASME PVP, Vol. **298** of *Flow Induced Vibrations*, ASME, pp. 37–43.

[6] Beale, S., and Spalding, D., 1999. "A numerical study of unsteady fluid flow in in-line and staggered tube banks". *Journal of Fluids and Structures,* ***13***, pp. 723–754.

[7] Sweeney, C., and Meskell, C., 2003. "Fast numerical simulation of vortex shedding in tube arrays using a discrete vortex method". *Journal of Fluids and Structures,* ***18***, pp. 501–512.

[8] Achenbach, E., 1969. "Investigations on the flow through a staggered tube bundle at reynolds numbers up to re=10^7". *Warmë und Stoffübertragung,* ***Bd 2***, pp. 47–52.

[9] Zdravkovich, M. M., and Namork, J. E., 1980. "Excitation, amplification and suppression of flow-induced vibration in heat exchangers.". *Proceedings Practical Experiences with Flow Induced Vibrations,* ***Paper A5***, pp. 107–117.

[10] Zukauskas, A. A., Ulinskas, R. V., and Bubelis, E. S., 1983. "Heat transfer in separated flows at re between 1 and 2.10^6 and pr between 0.7 and 10,000 (separation of vortices from tubes)". *Heat Transfer - Soviet Research,* ***15***(2), pp. 73–80.

[11] Batham, J. P., 1973. "Pressure distribution on in-line tube arrays in cross flow". *International Symposium, Vibration Problems in Industry, Keswick, U.K.,* ***Paper No. 411***, pp. 1–24.

[12] Mahon, J., and Mekell, C., 2009. "Surface pressure distribution survey in normal triangular tube arrays". *Journal of Fluids and Structures,* ***25***, pp. 1348–1368.

[13] Mahon, J., 2008. "Interaction between acoustic resonance and fluidelastic instability in a normal triangular tube arrays". *PhD Thesis*.

[14] Zukauskas, A., 1989. "Cylinders in crosflow". *High-Performance Single-Phase Heat Exchangers, Hemisphere Publishing Corporation,* ***Chapter 10***, pp. 187–206.

[15] Zdravkovich, M. M., and Stonebanks, K. L., 1990. "Intrinsically nonuniform and metastable flow in and behind tube arrays". *Journal of Fluids and Structures,* ***4***, pp. 305–319.

[16] Zdravkovich, M. M., 1993. "On suppressing metalstable interstitial flow behind a tube array". *Journal of Fluids and Structures,* ***7***(3), pp. 245–252.

[17] Mahon, J., Cheeran, P., and Meskell, C., 2010. "Spanwise correlations of pressure fluctuations in heat exchanger tube arrays". In ASME FEDSM 2010, ASME, pp. FEDSM–ICNMM2010–30483.